SPACE TIME METASURFACE
OPTIMISATION AND APPLICATIONS

Ng Le Xi[1], Chia Tse Tong[2]
[1]NUS High School, 20 Clementi Ave 1, Singapore 129957
[2]DSO National Laboratories, 12 Science Park Drive, Singapore 118225

Abstract

Space-time metasurfaces (STMs) are a class of metasurface that modulate in both space and time domains. They are capable of controlling the scattering of an incoming electromagnetic wave to its fundamental and harmonic frequencies, as well as manipulating the energy and momenta of the wave both reciprocally and nonreciprocally. Generating space-time matrix (STMx) that fulfil the specific requirements of the task at hand is the primary challenge associated with this field.

In this paper, we investigate the genetic optimization of an STMx in the near-field, far-field and oblique incidence cases to control the scattered direction and magnitude of a higher harmonic (of the modulation frequency) beam. We show that deflection of all harmonics up to 5th order is possible across the $\{-\frac{\pi}{2}, \frac{\pi}{2}\}$ angular range, as well as exhibiting some other possibilities for beam manipulation, and verify our results experimentally. This research can be extended to related fields, such as reflectarray antennae and time-modulated arrays.

Keywords: Space-time modulation, electromagnetics, metasurfaces

1. Introduction

A metasurface is an artificial surface constituting of an array of sub-wavelength scale periodic elements that can be used to manipulate incident electromagnetic waves. These surfaces have drawn growing attention from researchers in recent years, due to their ability to provide abrupt phase shift, as well as controlling (both steering and focusing) emitted wavefronts.

Electromagnetic (EM) wave manipulation plays a central role in many fields of science, from communications and wireless transmissions to optics and photonics. In this paper, we investigate a space-and-time-coding digital metasurface that enables manipulation of EM waves in both their propagation patterns, as well as their harmonic power distribution.

2. Theory

We can introduce the far-field E-field as a phasor sum of reflected rays from each element. We first define our surface as an $M \times N$ array of modulating elements, with elements at (p, q), with $x_{p+1} - x_p = d_x$, $y_{q+1} - y_q = d_y$, and reflection coefficients given as a space-time matrix $\Gamma_{pq}(t)$ with

$$\Gamma_{pq}(0) = A_{pq,0}\delta_{pq,0}$$

$$\Gamma_{pq}(1) = A_{pq,1}\delta_{pq,1}$$

$$\vdots$$

$$\Gamma_{pq}(T_0) = A_{pq,0}\delta_{pq,0}$$

where A and δ refer to the amplitude and phase of the modulated (p, q) element, respectively, and T_0 is the modulation period, after which the time cycle repeats. In the following section, we will investigate a solely phase modulated array.

We now impinge a plane wave normally on the array with wavenumber $k = \frac{2\pi}{\lambda_c}$. From an element at position (p, q) on the array, its scattered E-field in spherical coordinates is given by

$$E = E_{p,q}(\theta, \phi)\exp\{jk(pd_x \sin\theta\cos\phi + qd_y \sin\theta \sin\phi)\}$$

where $E_{p,q}(\theta, \phi)$ is the far-field pattern of the (p, q) element at the central frequency f_c. For simplicity, we set $E_{p,q}(\theta, \phi)$ to unity unless otherwise specified. Given the length of the time array as L and neglecting mutual coupling between the elements, the total scattered far-field pattern of the $M \times N$ STM array at the m^{th} harmonic frequency ($f_c + mf_0$, where f_0 is the modulation frequency) can then be written as [1]

$$E_m(\theta, \phi) = \sum_{q=0}^{N-1}\sum_{p=0}^{M-1} E_{p,q}(\theta, \phi)\exp\{jk_2(pd_x \sin\theta\cos\phi + qd_y \sin\theta \sin\phi)\}\sum_{b=1}^{L}\frac{\delta_{pq,b}}{\pi m}\sin[\frac{\pi m}{L}]e^{-\frac{j\pi m(2b-1)}{L}}$$

where k_2 is the wavenumber of the outgoing wave, given by $k_2 = \frac{2\pi(f_c+mf_0)}{c}$.

We may now plot the 3D scattering pattern for a few example matrices, with $\lambda = 3\ cm, d_x = d_y = 1.5\ cm,\ p = q = L = 8$. First, we demonstrate the scattering pattern of a diagonal matrix, with the main beam of the first harmonic offset from the normal as shown in Fig. 2.1.

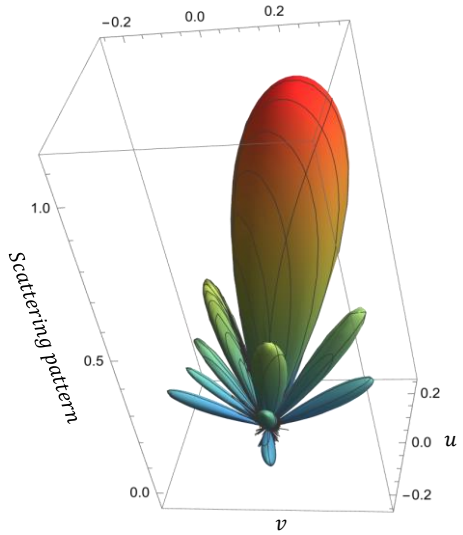

$$\text{Time} \quad \begin{pmatrix} 1 & 0 & 0 & 0 & 0 & 0 & 0 & 0 \\ 0 & 1 & 0 & 0 & 0 & 0 & 0 & 0 \\ 0 & 0 & 1 & 0 & 0 & 0 & 0 & 0 \\ 0 & 0 & 0 & 1 & 0 & 0 & 0 & 0 \\ 0 & 0 & 0 & 0 & 1 & 0 & 0 & 0 \\ 0 & 0 & 0 & 0 & 0 & 1 & 0 & 0 \\ 0 & 0 & 0 & 0 & 0 & 0 & 1 & 0 \\ 0 & 0 & 0 & 0 & 0 & 0 & 0 & 1 \end{pmatrix} \text{Space}$$

Fig 2.1: 3D scattering pattern of the first harmonic for given Γ.

We can also generate "vortex beams" with a 4-phase states STM as shown in Fig. 2.2, with the phase circulating around the centre of the beam.

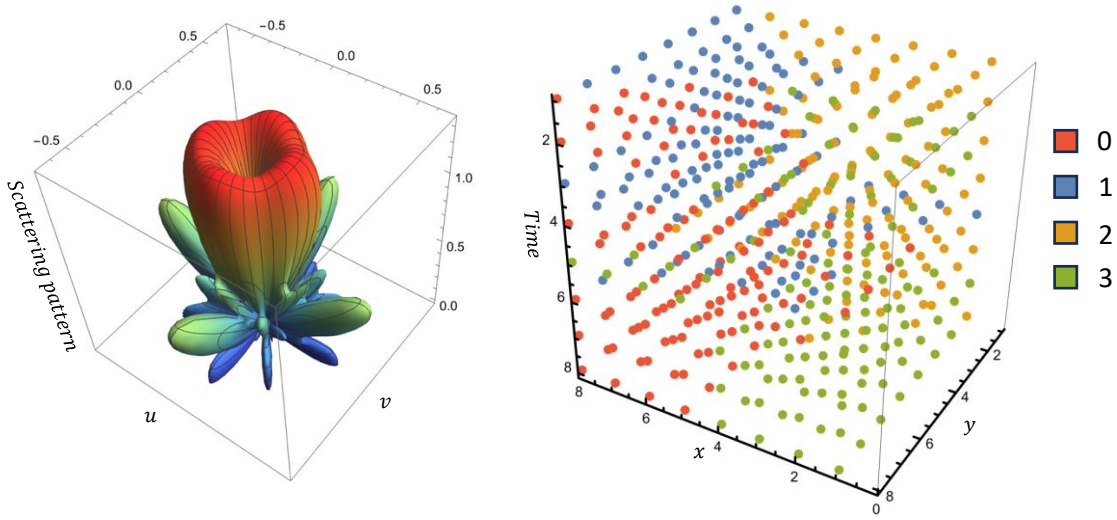

Fig 2.2: Vortex beam generation with a (2 bit or) 4 phase-state STM.

3. Optimization of STMx

In order to improve the metasurface's applicability, we now tailor the metasurface to fulfil specific requirements. In particular, we seek to deflect the main beam of a certain harmonic to a specific angle, while suppressing its sidelobes and all other harmonics. Noting that this problem is difficult to solve analytically due to the large (x^n) space of solution, we introduce a genetic algorithm for optimization. We use a μ+λ-GA (genetic algorithm using a population of size μ and recombination pool of size λ) [2], with fitness defined as

$$4\sum_i \left(x_{p_i} - x_{p_i,0}\right) - \max\left(p_1, \ldots, p_i, \mathrm{i} \neq \mathrm{i}_{\mathrm{shift}}\right)$$

where $x_{p_{i,0}}$ refers to the target positions of the shifted peaks, with the second term designed to lower all other peaks and reduce sidelobes, and the factor 4 being a weighting constant to emphasize beam steering over sidelobe suppression.

Fig. 3. 1 shows the flowchart of the genetic algorithm. The initial generation of matrices is randomly generated, and uniformly distributed in the 64-space (for an 8×8 array). The above fitness function is then applied to them, and parents are selected via roulette selection. "Child" matrices are generated via crossover of parent matrices, as well as low probability bitflip "mutations." The remaining lowest fitness members are removed to maintain the initial population size. This cycle repeats until the maximum fitness exceeds a specified threshold or the maximum number of generations is reached, and the optimized matrix is generated.

After testing, we set the hyperparameters of optimisation as follows:

- replacement rate = 0.25,
- mutation rate = 0.05,
- crossover probability = 0.9, and
- initial population size = 100.

We reach convergence in about 200 generations in general, with each complete run taking less than 30min to plateau (see Fig. 3.2).

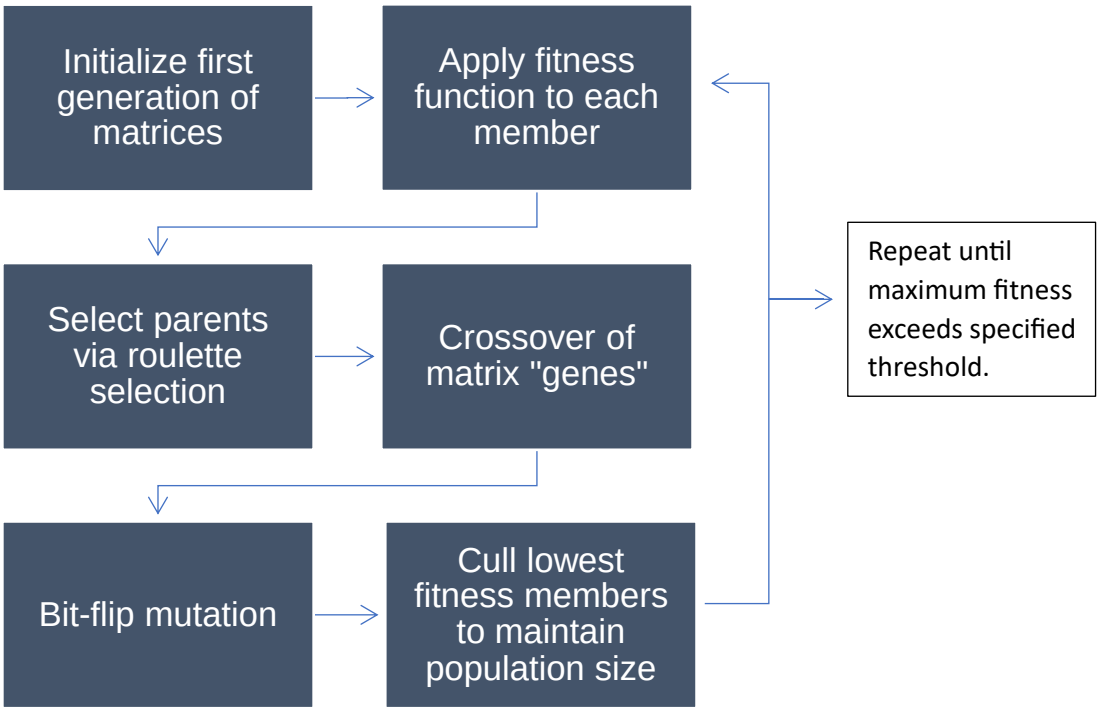

Fig 3.1: Flowchart of genetic algorithm.

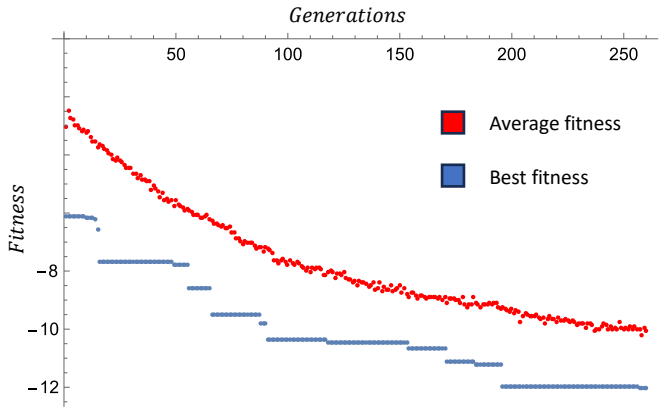

Fig 3.2: Fitness of population against generation.

We use a (1,8,8) 2-bit STMx linear array in the following examples. Using 2 bits, we generate STM for beam steering and sidelobe suppression. A few examples of this capability are shown below (all plots are cuts along the $\phi = 0$ axis). In Fig 3.3, we shift the 0^{th} harmonic (i.e., the fundamental frequency) to $\theta = 10°$, while in Fig 3.4, we shift the 2^{nd} harmonic to $\theta = 30°$, all while suppressing the other harmonics and sidelobes.

We may also generate STMs fulfilling more obscure demands by tweaking the fitness function. We can steer multiple peaks simultaneously (see Fig. 3.5) or reduce all peaks to a uniform level (Fig. 3.6).

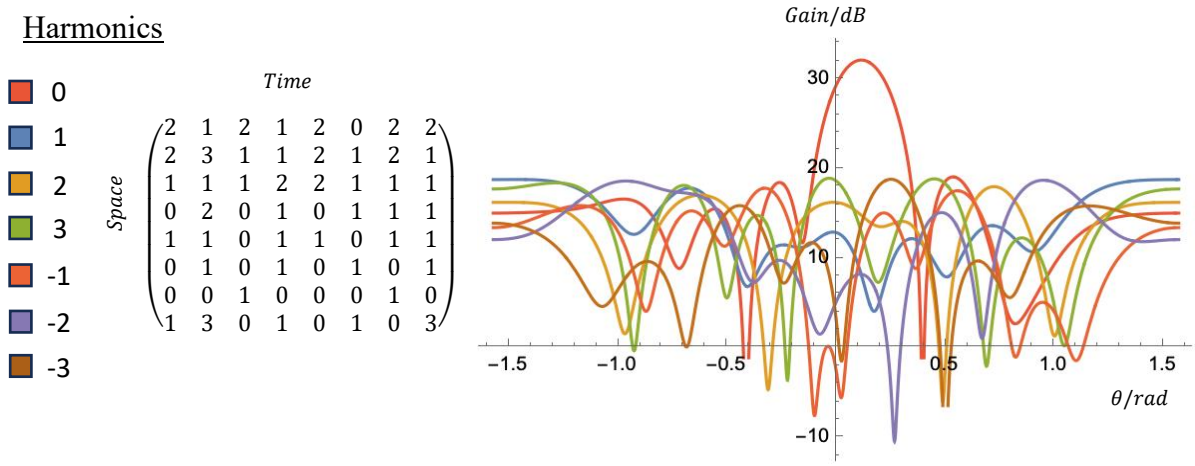

Fig. 3.3: An optimised STMx for deflection of the 0th harmonic main beam to $+\frac{\pi}{18} rad$ (10°).

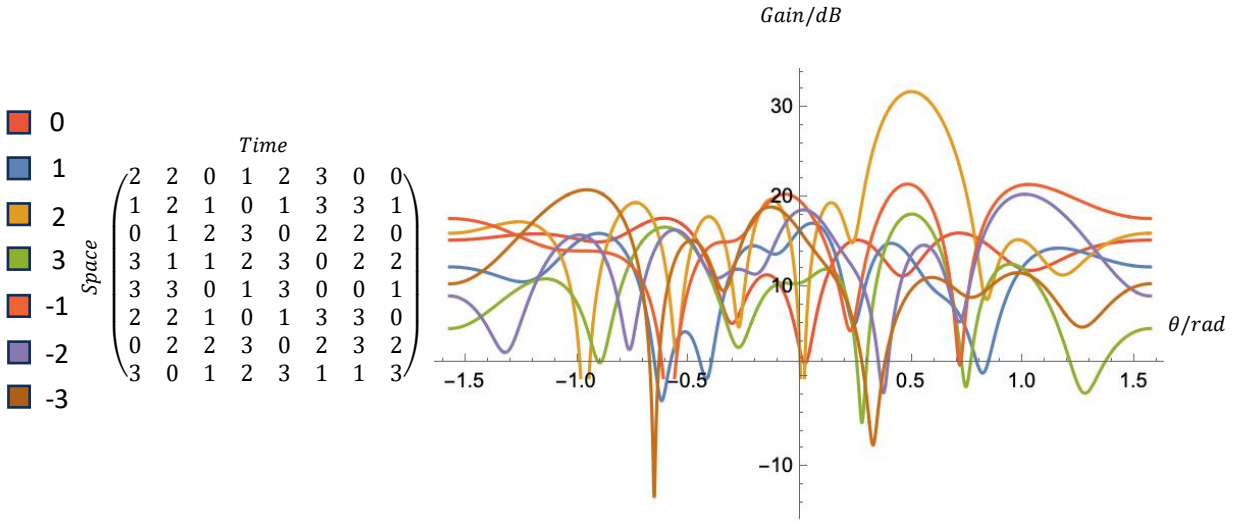

Fig. 3.4: An optimized STMx for deflection of the 2nd harmonic to $+\frac{\pi}{6} rad$ (30°).

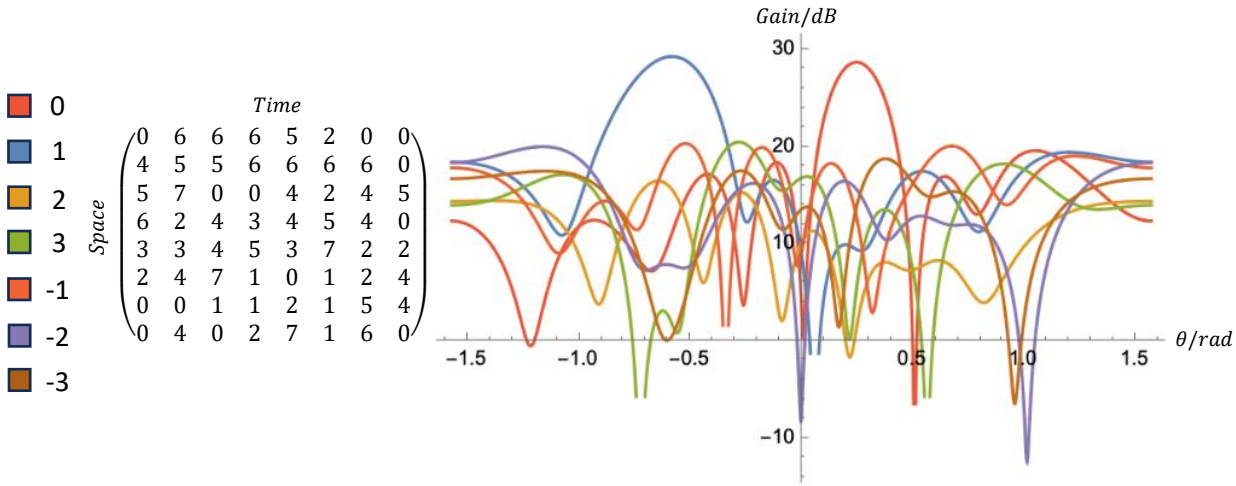

Fig. 3.5: A STM deflecting the 0th harmonic to $+15°$ and the 1st harmonic to $-30°$.

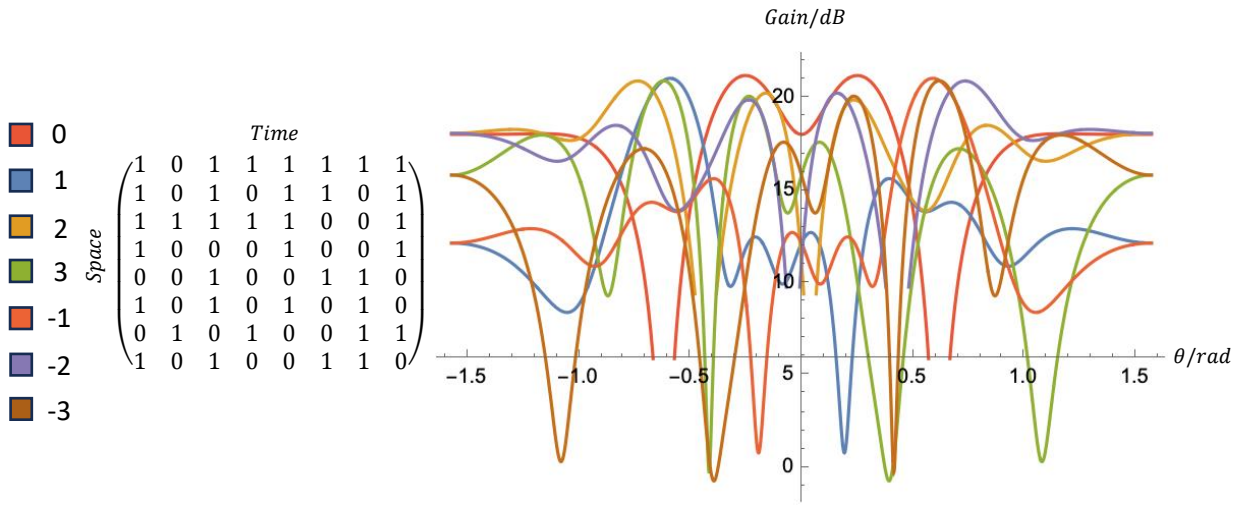

Fig. 3.6: A STM making all harmonics uniform in peak gain.

Interestingly, there seem to be many local maxima for each problem. If we take the Frobenius norm of each STMx generated for a single problem, we find that they are essentially randomly distributed throughout the 64-space, even with each matrix being functionally identical in far-field pattern generated (see Fig. 3.7 for example).

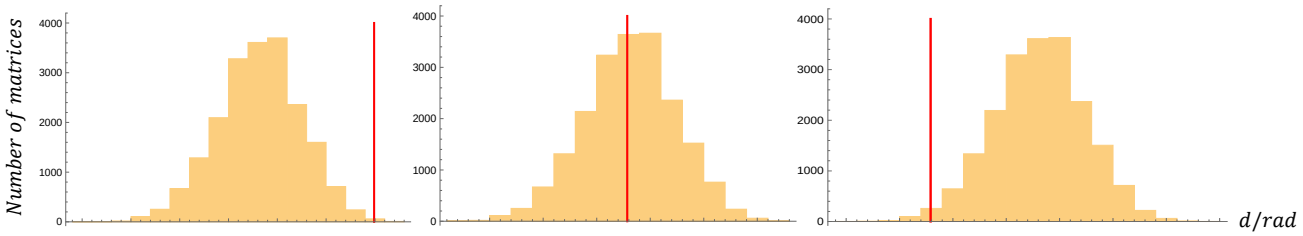

Fig 3.7: A comparison of the positions of 3 matrices (red line) from a control matrix (optimised for 30° deflection of 1st harmonic) in 64-space, showing that they are significantly different.

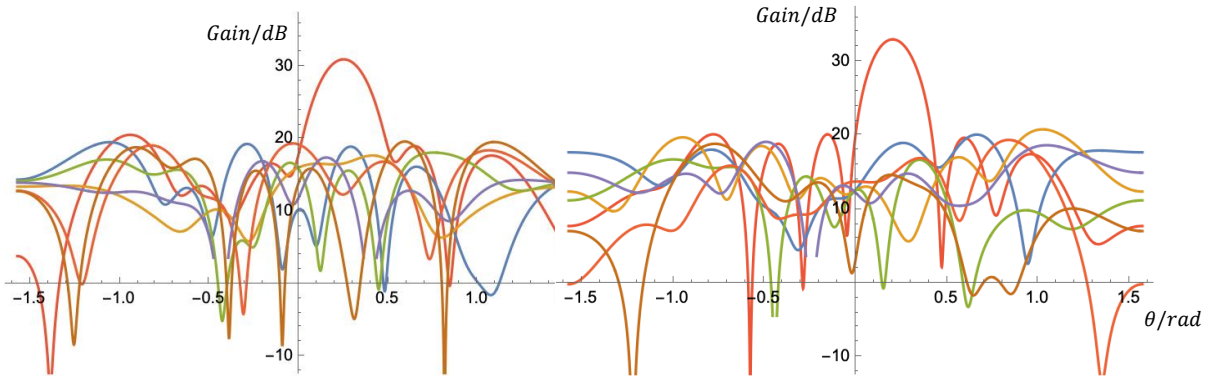

Fig 3.8: A comparison of far-field scattering pattern for the 1st and 3rd matrices of Fig. 3.7.

We also note that the efficacy of this optimisation can be improved with increased number of bits or elements, as seen in Fig 3.9, where increasing bits speeds up convergence and slightly increases final fitness. This is due to the increased resolution of the phase space and thus greater control over beam steering. In fact, as the number of elements and bits goes to infinity (a continuous metasurface), we can achieve 100% energy throughput efficiency. Of course,

this is unrealistic in a practical scenario, so we shall restrict our discussion to relatively small metasurfaces, with time and space lengths less than 10 elements.

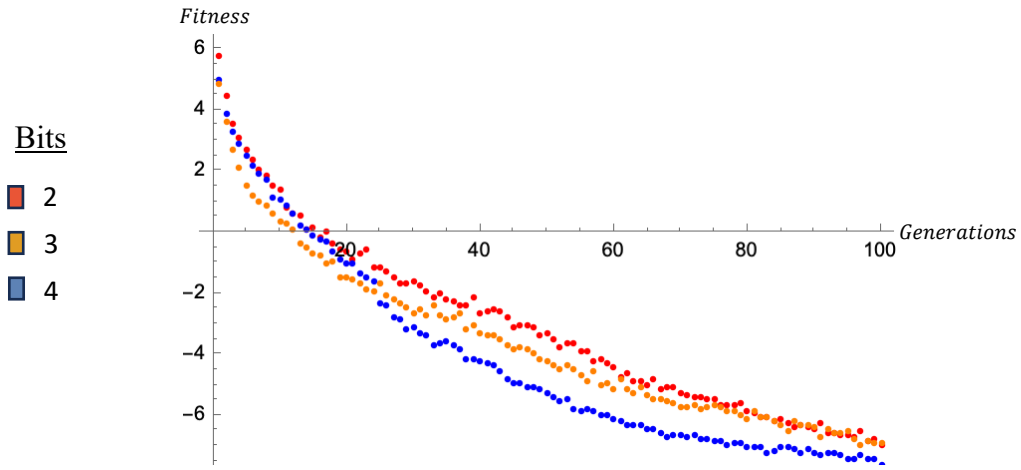

Fig 3.9: Comparison of convergence rates for 2-bit, 3-bit and 4-bit optimizations.

4. Oblique incidence

If the plane wave is not incident normally upon the metasurface, we can modify the outgoing distance phasor term in the scattering pattern of the m^{th} harmonic to obtain the following,

$$E_m(\theta,\phi) = \sum_{q=0}^{N-1}\sum_{p=0}^{M-1} E_0(\theta)\exp\{jk_1(pd_x\sin\theta_i\cos\phi_i + qd_y\sin\theta_i\sin\phi_i) + jk_2(pd_x\sin\theta\cos\phi + qd_y\sin\theta\sin\phi)\}\sum_{b=1}^{L}\frac{\delta_{pqb}}{\pi m}\sin[\frac{\pi m}{L}]e^{-\frac{j\pi m(2b-1)}{L}}$$

where the incident plane wave is at angle (θ_i, ϕ_i), the wavenumber of the incident wave is $k_1 = \frac{2\pi f_1}{c}$, and the wavenumber of the outgoing wave is $k_2 = \frac{2\pi f_2}{c}$, where $f_2 = f_1 + mf_0$ and f_0 is the modulation frequency.

Optimised matrices for this system may be obtained by direct genetic optimisation (as above), or phase-shifting an already optimised matrix for normal incidence as such for $\phi_i = 0$ (however, this may result in quantisation errors depending on bit resolution):

$$\Gamma_{oblique} = \Gamma_{normal} + \begin{pmatrix} 0 & d_x\sin\theta_i & \cdots & (N-1)d_x\sin\theta_i \\ \vdots & \vdots & \ddots & \vdots \\ 0 & d_x\sin\theta_i & \cdots & (N-1)d_x\sin\theta_i \end{pmatrix}$$

The asymmetry of this system allows for some interesting nonreciprocal effects [3]. If a plane wave is impinged upon the STM at $\theta = +60°$, with modulation frequency of 250 MHz, incident wave frequency of 5 GHz, and $d = \frac{\lambda}{2}$, the 1st harmonic (5.25 GHz) of the outgoing wave is at $\theta = -20.3°$. However, when a plane wave at 5.25 GHz is incident at $\theta = -20.3°$, the outgoing 1st harmonic (5.5 GHz) dominant beam is instead deflected to $\theta = +51.2°$ as shown in Fig. 4.1.

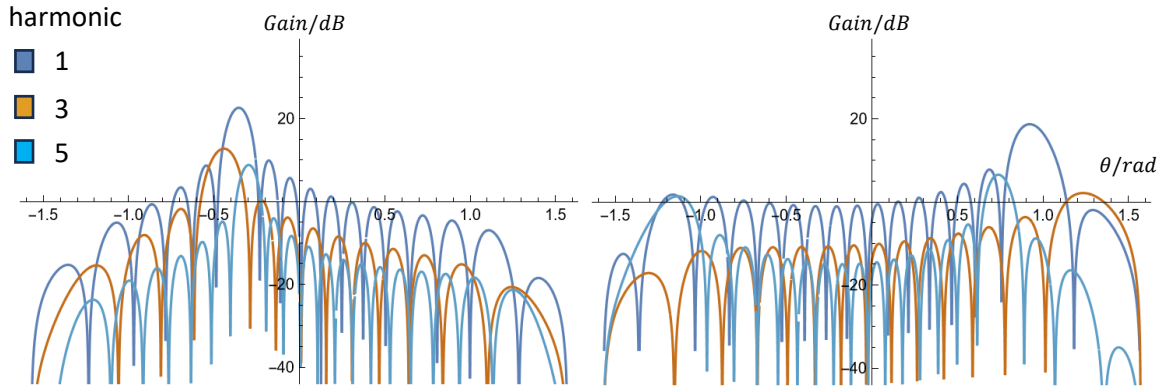

Fig 4.1: Nonreciprocity of metasurface: incident angle $\theta = 60°$ (L) and $\theta = -20.3°$ (R).

5. Near-field incidence

In many applications, we may be interested in the case where the incoming wave is from a relatively nearby source and is reflected to form the received far-field pattern. For this near-field incidence case (where the wave arrives as a spherical rather than a plane wave) we may handle the reflection by simply adding a phase constant dependent on the distance of the array element from the beam source. Then, the far-field scattering pattern can be written as follows, with $\vec{r}$ being the position of the beam source relative to the array:

$$E(\theta,\phi) = \sum_{q=0}^{N-1}\sum_{p=0}^{M-1} E_0(\theta)\exp\{jk_1|\vec{r} - \begin{pmatrix} pd_x \\ qd_y \\ 0 \end{pmatrix}|\}\exp\{jk_2(pd_x \sin\theta\cos\phi + qd_y \sin\theta \sin\phi)\}\sum_{b=1}^{L}\frac{A_{pqb}\delta_{\mathrm{pqb}}}{\pi m}\sin[\frac{\pi m}{L}]e^{-\frac{j\pi m(2b-1)}{L}}$$

As an example, we set the beam source location at 1.67λ above the centre of the metasurface. We can then rerun the optimization and obtain optimized matrices and scattering patterns for this new scenario (see Fig. 5.1). Alternatively, similarly to the above scenario of oblique incidence, we can modify an optimised matrix for normal incidence via adding a phase-shift constant to each element given by:

$$\delta_{shift} = k_1\left|\vec{r} - \begin{pmatrix} pd_x \\ qd_y \\ 0 \end{pmatrix}\right|$$

We find that these optimised STMx approach approximately with equal efficiency (fitness-wise) as in the first scenario, which is intuitive.

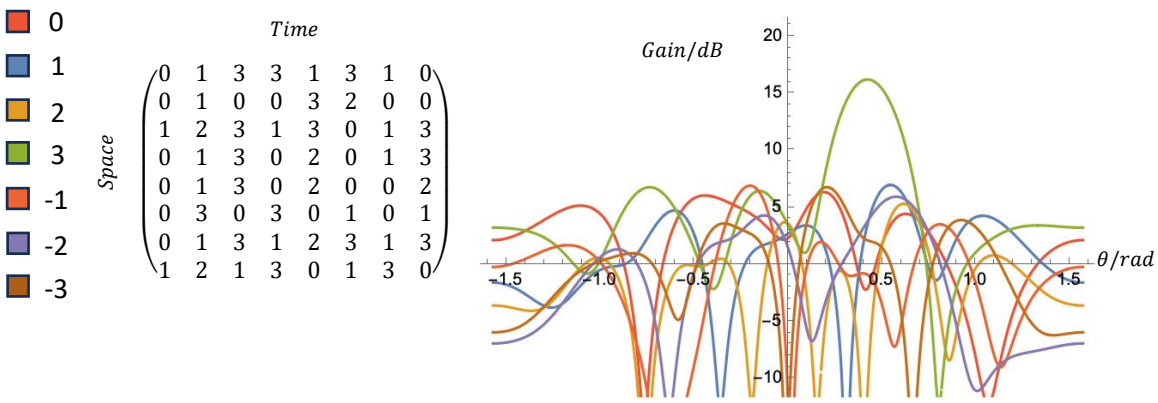

Fig 5.1: A metasurface steering the 3rd harmonic in the $+60°$ direction (near-field)

6. Extension to reflectarray antennas

We can apply the same method to the optimisation of the phase settings for reflectarray antennas. As the phase-shift is now time-invariant, the far field scattering pattern simplifies to:

$$E(\theta,\phi) = \sum_{q=0}^{y}\sum_{p=0}^{x} A_{pq}\delta_{\mathrm{pq}}E_0(\theta)\exp\{jk\left|\vec{r} - \begin{pmatrix} pd_x \\ qd_y \\ 0 \end{pmatrix}\right| \times \exp\{jk(pd_x \sin\theta\cos\phi + qd_y \sin\theta\sin\phi)\}$$

In reflectarray antennas, it is often desired that the edge taper is about 10dB. Hence, we modify $E_0(\theta) = |E_0|\cos^e \alpha_i$, where α_i is the angle between the incident beam and the reflectarray element and e is the power factor of the pattern to match the desired edge taper.

Similar to above, we would like to both control sidelobes and steer the main beam of the reflected field. Unlike the STM, an analytic solution for beam steering is readily available as:

$$\delta_{xy} = k[d_i - \sin\theta_d\,(x_i\cos\phi_d + y_i\sin\phi_d)]$$

where $\{\theta_d, \phi_d\}$ is the desired beam steering angle. However, this does not take sidelobes into account, which may be unnecessarily large and reduce the energy throughput of the main beam. To rectify this, we can simply rerun the same genetic algorithm used above, with the initial population consisting of 8 by 8 matrices that fulfil the above condition. This significantly speeds up optimisation, and we end up with a satisfactory solution in under 80 generations (see Fig. 6.2). In Fig. 6.1, we can see that an unoptimized matrix has its main beam in the correct direction but has significant sidelobes that reduce its gain (~28dB), while the optimised matrix has significantly reduced sidelobes and increased gain (~32dB).

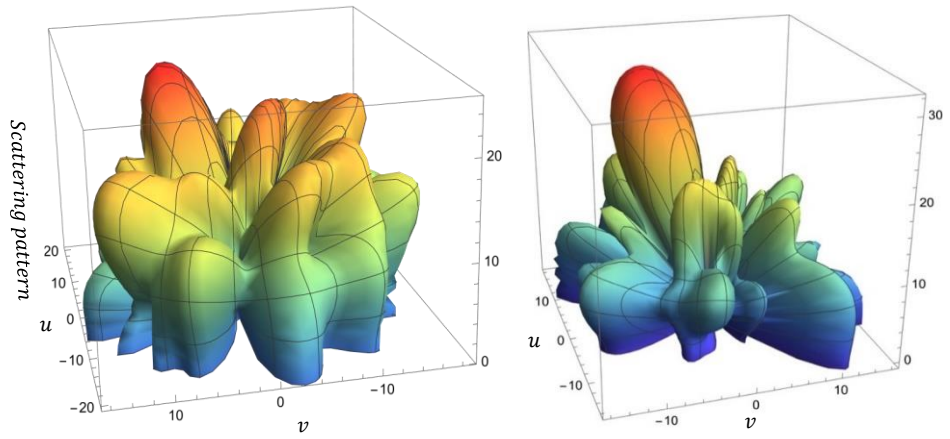

Fig 6.1: Comparison of radiation patterns of unoptimized and optimized reflectarray antenna.

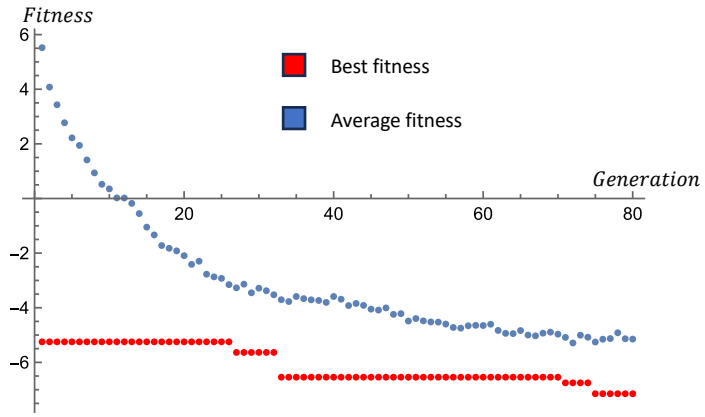

Fig 6.2: Convergence of reflectarray antenna optimisation

7. Extension to time-modulated linear arrays

Time-modulated linear arrays (TMLAs) are binary amplitude-modulated arrays controlled by the application of variable width electronic pulses to the array elements. Hence, in the usual case where the pulse lengths are a divisor of the total time sequence length, the system behaviour is essentially identical to that of a 1-bit amplitude modulated STM. We can thus apply the same techniques as above. The most common application of TMLAs is for efficient sidelobe suppression without the use of phase-switching. We demonstrate this capability below by optimising an 8-domain array with time matrix length 8.

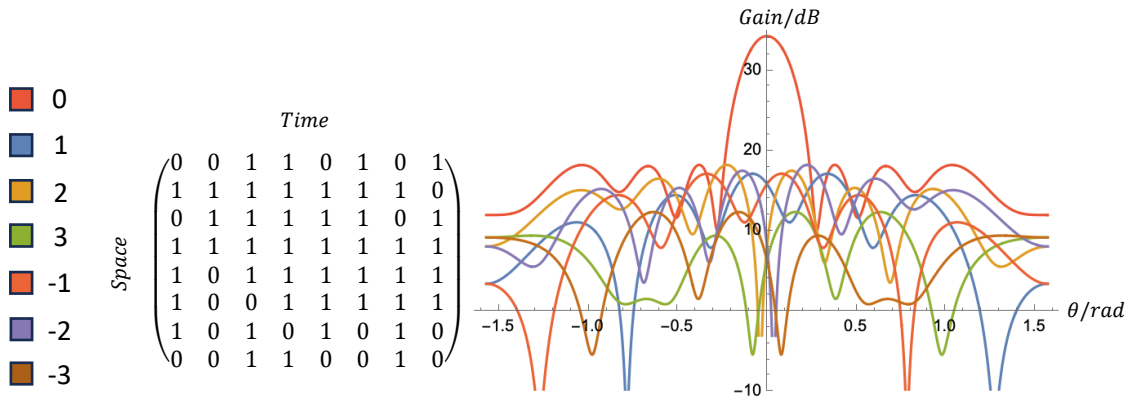

Fig 7.1: Sidelobe suppression with optimised time-modulated linear array

8. Experimental verification

To verify the above results, we run an experiment based on a simulated version of the space-time metasurface via a time-modulated array.

8.1 Experimental Design

The experiment is setup is as shown in Fig. 8.1.1.

Fig 8.1.1: Experimental set-up in office space. (L) Complete view of setup. (Top-R) View of STM array and its RF backend, power supply and controller. (Bottom-R) Receiving end with receive horn connected to spectrum analyser.

The following simulated metasurfaces were tested:

Test case	Matrix (x: space; y: time)	Notes
1	$\begin{pmatrix} 2 & 2 & 1 & 1 & 0 & 0 & 3 & 2 \\ 2 & 1 & 1 & 0 & 0 & 3 & 2 & 3 \\ 2 & 2 & 1 & 1 & 1 & 0 & 3 & 3 \\ 2 & 1 & 1 & 1 & 0 & 0 & 0 & 2 \\ 1 & 2 & 1 & 0 & 3 & 0 & 3 & 2 \\ 2 & 2 & 2 & 1 & 0 & 3 & 3 & 2 \\ 3 & 1 & 1 & 0 & 0 & 3 & 3 & 3 \\ 2 & 1 & 0 & 0 & 0 & 3 & 3 & 3 \end{pmatrix}$	Steering of fundamental harmonic to +15°
2	$\begin{pmatrix} 0 & 0 & 0 & 0 & 3 & 3 & 2 & 2 \\ 0 & 0 & 0 & 0 & 0 & 0 & 3 & 3 \\ 1 & 1 & 0 & 0 & 0 & 0 & 0 & 0 \\ 2 & 1 & 1 & 1 & 0 & 0 & 0 & 0 \\ 2 & 2 & 2 & 1 & 1 & 1 & 1 & 0 \\ 3 & 2 & 2 & 2 & 2 & 1 & 1 & 1 \\ 3 & 3 & 3 & 2 & 2 & 2 & 2 & 1 \\ 0 & 0 & 3 & 3 & 3 & 2 & 2 & 2 \end{pmatrix}$	Steering of 1st harmonic to +7.5°
3	$\begin{pmatrix} 1 & 1 & 3 & 1 & 3 & 2 & 1 & 0 \\ 3 & 0 & 3 & 1 & 0 & 3 & 3 & 3 \\ 3 & 1 & 3 & 3 & 1 & 3 & 2 & 0 \\ 2 & 2 & 0 & 0 & 1 & 0 & 3 & 1 \\ 0 & 2 & 0 & 3 & 2 & 0 & 3 & 1 \\ 3 & 3 & 0 & 0 & 3 & 1 & 3 & 2 \\ 1 & 0 & 1 & 1 & 3 & 2 & 0 & 3 \\ 0 & 0 & 2 & 2 & 3 & 1 & 0 & 1 \end{pmatrix}$	Oblique incidence at -30°, steering of 1st harmonic to +15°
4	$\begin{pmatrix} 1 & 2 & 1 & 0 & 3 & 3 & 3 & 3 \\ 3 & 1 & 1 & 0 & 0 & 0 & 1 & 2 \\ 3 & 2 & 1 & 2 & 1 & 0 & 0 & 3 \\ 2 & 3 & 2 & 3 & 1 & 1 & 1 & 0 \\ 0 & 3 & 2 & 2 & 2 & 1 & 1 & 0 \\ 3 & 0 & 2 & 3 & 3 & 2 & 1 & 1 \\ 1 & 1 & 3 & 0 & 3 & 3 & 2 & 2 \\ 0 & 1 & 0 & 1 & 3 & 2 & 2 & 0 \end{pmatrix}$	Test case 3 uncorrected for oblique incidence (assuming normal incidence)

8.2 Experimental Results

We find that the experimental results match extremely well with the theoretical model, with most of the measured relative amplitudes of harmonics at projected angles deviating from the predicted values by less than 0.1, which is less than experimental error (Fig 8.2). We were also able to observe beam steering in the expected directions, verifying the effectiveness of this process.

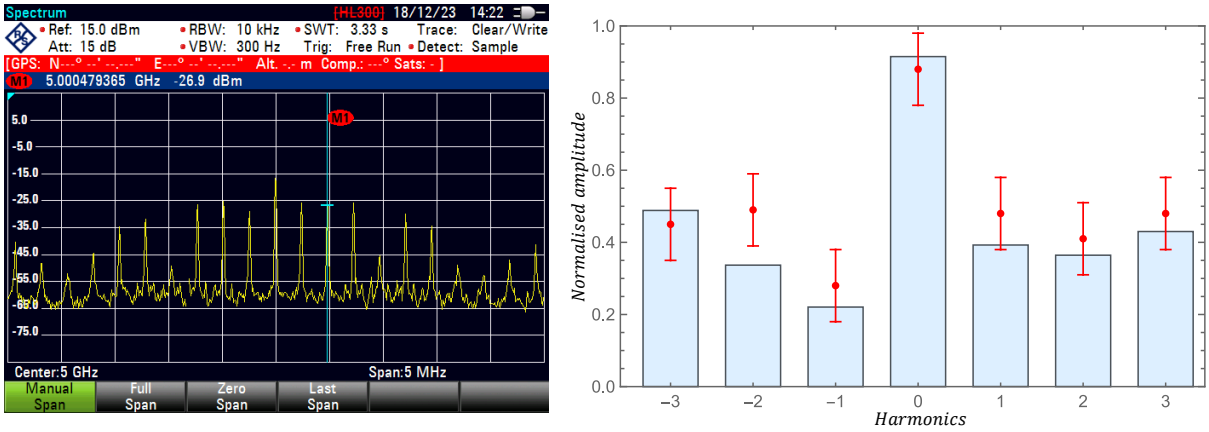

Fig 8.2.1: Harmonic power distribution (L) and comparison between predicted and experimental harmonic amplitudes (R) for case 1.

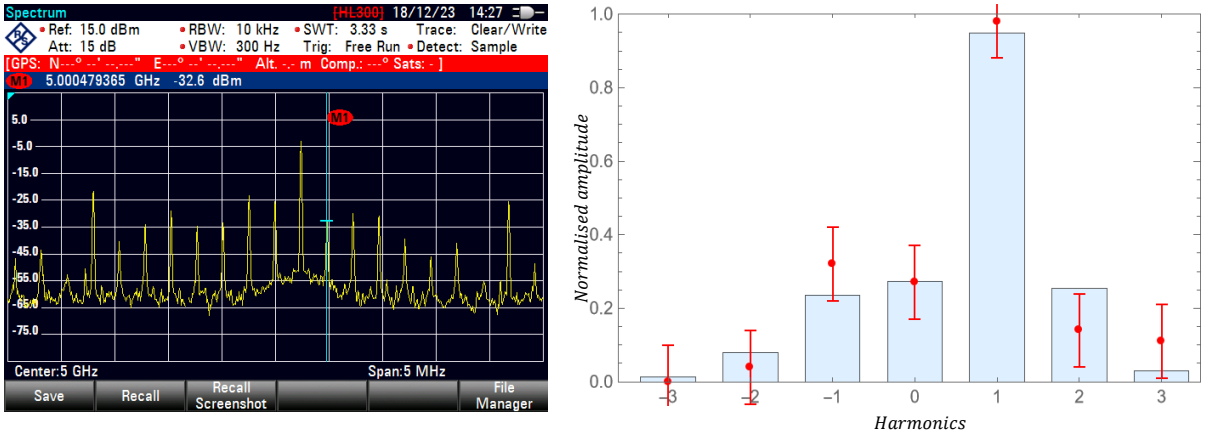

Fig 8.2.2: Harmonic power distribution (L) and comparison between predicted and experimental harmonic amplitudes (R) for case 2.

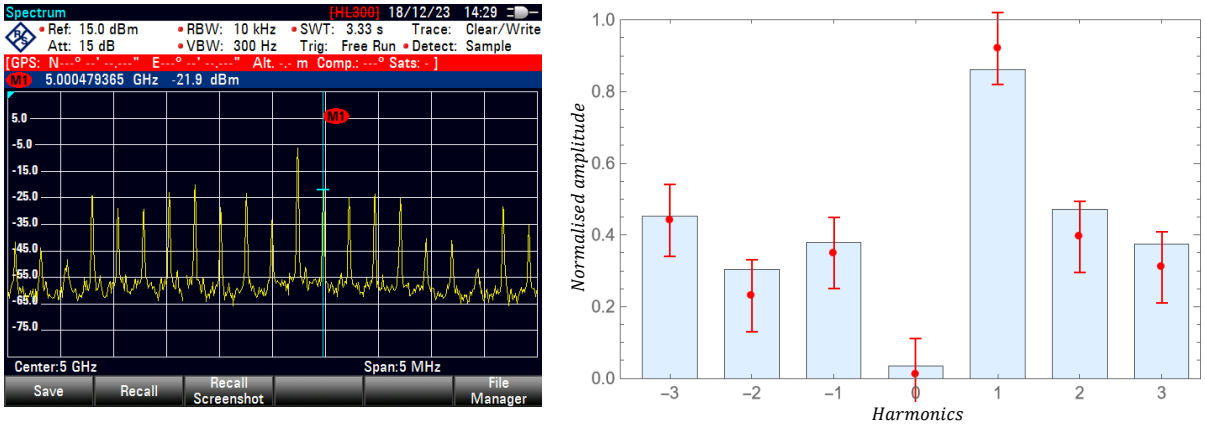

Fig 8.2.3: Harmonic power distribution (L) and comparison between predicted and experimental harmonic amplitudes (R) for case 3.

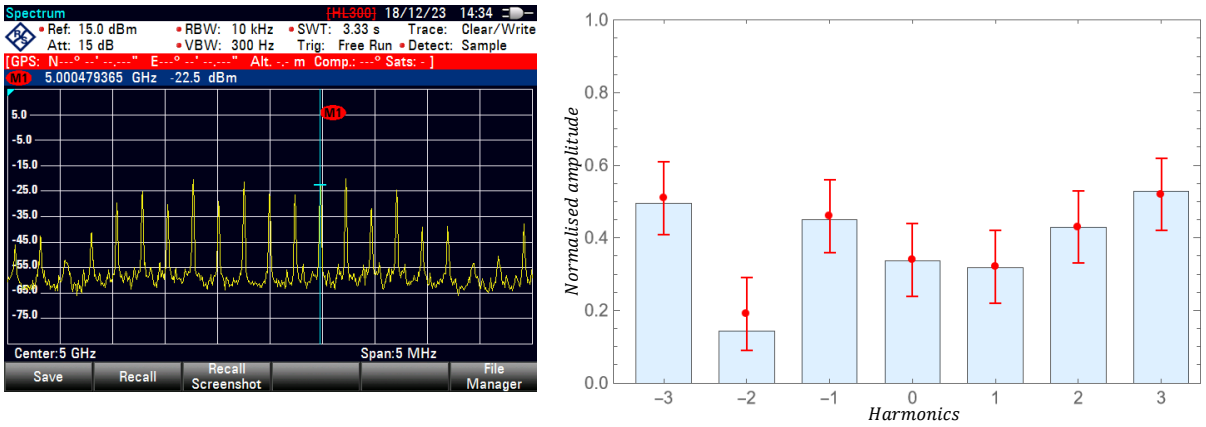

Fig 8.2.4: Harmonic power distribution (L) and comparison between predicted and experimental harmonic amplitudes (R) for case 4.

9. Conclusion

We have demonstrated the capabilities of STM for beam steering and suppression of sidelobes and harmonics in both the near-field and far-field incidence cases using genetic optimisation, verifying the theoretical results with an experimental prototype, as well as proved the applicability of this method in related fields such as reflectarray antennae and time-modulated arrays.

Acknowledgements

I would like to thank Dr Chia Tse Tong for his invaluable support and guidance throughout this project. I would also like to thank Dr Chio Tan Huat (DSO) and Mr Cheng Jang Ming (Temasek Laboratories @ NUS) for supplying hardware and setting up the experimental apparatus. Finally, I would like to thank DSO National Laboratories for giving me the opportunity to take up this project.

References

1. Zhang, L., Chen, X.Q., Liu, S. *et al.* Space-time-coding digital metasurfaces. Nat Commun 9, 4334 (2018). https://doi.org/10.1038/s41467-018-06802-0
2. Slowik, A., Kwasnicka, H. Evolutionary algorithms and their applications to engineering problems. Neural Comput & Applic 32, 12363–12379 (2020). https://doi.org/10.1007/s00521-020-04832-8
3. Yang, W., Qin, J., Long, J. *et al.* A self-biased non-reciprocal magnetic metasurface for bidirectional phase modulation. *Nat Electron* 6, 225–234 (2023). https://doi.org/10.1038/s41928-023-00936-w

Appendix 1

Derivation of scattering pattern for phase-modulated STMx:

$$E(\theta,\phi)=\sum_{q=0}^{n}\sum_{p=0}^{m}\Gamma_{pq}(t)E_0(\theta,\phi)\exp\{jk(pd_x\sin\theta\cos\phi+qd_y\sin\theta\sin\phi)\}$$

Where $\Gamma_{pq}(t)$ is the time-modulated reflection coefficient of the (p,q) element. It is assumed to be a periodic function of time, defined over one period as a linear combination of shifted pulse functions as follows:

$$\Gamma_{pq}(t)=\sum_{n=1}^{L}\Gamma_{pq}^{n}\mathrm{U}_{pq}^{n}(t)\,,(0<\mathrm{t}<T_0)$$

where $\mathrm{U}_{pq}^{n}(t)$ is a periodic pulse function with modulation period T_0. $\Gamma_{pq}^{n}=\mathrm{A}_{pq}^{n}\exp(j\phi_{pq}^{n})$ is the reflection coefficient of the (p,q) element during the interval $(n-1)\tau\le t\le n\tau$ at the central frequency, where A_{pq}^{n} and ϕ_{pq}^{n} denote the amplitude and phase, respectively.

In each period T_0,

$$\mathrm{U}_{pq}^{n}(t)=\begin{cases}1,(n-1)\tau\le t\le n\tau\\0,\text{otherwise}\end{cases}$$

To remove the time dependence, we may then convert Γ to a Fourier sum in harmonics of the main beam:

$$\begin{aligned}\Gamma&=\sum_{n=1}^{L}\Gamma_{pq}^{n}\int_{(n-1)\tau}^{n\tau}e^{-2\pi imf_o t}\,dt\\&=\sum_{n=1}^{L}\Gamma_{pq}^{n}\int_{\frac{(n-1)\tau}{T_0}}^{\frac{n\tau}{T_0}}e^{-2\pi imu}\,du\\&=\sum_{n=1}^{L}\Gamma_{pq}^{n}\int_{\frac{(n-1)}{L}}^{\frac{n}{L}}e^{-2\pi imu}\,du\\&=\sum_{n=1}^{L}\frac{\Gamma_{pq}^{n}}{\pi m}\sin[\frac{\pi m}{L}]e^{-\frac{i\pi m(2b-1)}{L}}\end{aligned}$$

And as such, derive the expression for the E-field as above:

$$\begin{aligned}E(\theta,\phi)=\sum_{q=0}^{N}\sum_{p=0}^{M}E_0(\theta)\exp\{jk(pd_x\sin\theta\cos\phi\\+qd_y\sin\theta\sin\phi)\}\sum_{b=1}^{L}\frac{A_{pq,b}\delta_{pq,b}}{\pi m}\sin[\frac{\pi m}{L}]e^{-\frac{j\pi m(2b-1)}{L}}\end{aligned}$$

Appendix 2

Time cuts of vortex beam STMx (t=1 to 8) for Fig. 2.2.

$$\begin{pmatrix} 2&2&2&2&2&2&2&1\\ 2&2&2&2&2&2&1&1\\ 2&2&2&2&2&1&1&1\\ 2&2&2&2&1&1&1&1\\ 3&3&3&3&0&1&1&1\\ 3&3&3&0&0&0&1&1\\ 3&3&0&0&0&0&0&1\\ 3&0&0&0&0&0&0&0 \end{pmatrix} \begin{pmatrix} 2&2&2&2&1&1&1&1\\ 3&2&2&2&1&1&1&1\\ 3&3&2&2&1&1&1&1\\ 3&3&3&2&1&1&1&1\\ 2&2&2&2&0&0&0&0\\ 2&2&2&3&0&0&0&0\\ 2&2&3&3&0&0&0&0\\ 2&3&3&3&0&0&0&0 \end{pmatrix} \begin{pmatrix} 2&2&2&2&2&2&2&1\\ 3&2&2&2&2&2&1&1\\ 3&3&2&2&2&1&1&1\\ 3&3&3&2&1&1&1&1\\ 3&3&3&3&1&1&1&1\\ 3&3&3&0&1&1&1&1\\ 3&3&0&0&1&1&1&1\\ 3&0&0&0&1&1&1&1 \end{pmatrix} \begin{pmatrix} 2&2&2&2&1&1&1&1\\ 2&2&2&2&1&1&1&1\\ 2&2&2&2&1&1&1&1\\ 2&2&2&2&1&1&1&1\\ 0&0&0&0&0&1&1&1\\ 0&0&0&0&0&0&1&1\\ 0&0&0&0&0&0&0&1\\ 0&0&0&0&0&0&0&0 \end{pmatrix}$$

$$\begin{pmatrix} 1&1&1&1&2&2&2&1\\ 2&1&1&1&2&2&1&1\\ 2&2&1&1&2&1&1&1\\ 2&2&2&1&1&1&1&1\\ 3&3&3&3&3&0&0&0\\ 3&3&3&0&3&3&0&0\\ 3&3&0&0&3&3&3&0\\ 3&0&0&0&3&3&3&3 \end{pmatrix} \begin{pmatrix} 2&2&2&2&2&2&2&2\\ 2&2&2&2&2&2&2&2\\ 2&2&2&2&2&2&2&2\\ 2&2&2&2&2&2&2&2\\ 3&3&3&3&0&1&1&1\\ 3&3&3&3&0&0&1&1\\ 3&3&3&3&0&0&0&1\\ 3&3&3&3&0&0&0&0 \end{pmatrix} \begin{pmatrix} 3&3&3&3&1&1&1&1\\ 3&3&3&3&1&1&1&1\\ 3&3&3&3&1&1&1&1\\ 3&3&3&3&1&1&1&1\\ 3&3&3&3&0&0&0&0\\ 3&3&3&3&0&0&0&0\\ 3&3&3&3&0&0&0&0\\ 3&3&3&3&0&0&0&0 \end{pmatrix} \begin{pmatrix} 2&2&2&2&1&1&1&0\\ 3&2&2&2&1&1&0&0\\ 3&3&2&2&1&0&0&0\\ 3&3&3&2&0&0&0&0\\ 3&3&3&3&0&0&0&0\\ 3&3&3&3&0&0&0&0\\ 3&3&3&3&0&0&0&0\\ 3&3&3&3&0&0&0&0 \end{pmatrix}$$